Identification of vacuolar phosphate influx transporters in Brassica napus

Bei Han[1], Chuang Wang[2], Tao Wu[1], Junjun Yan[1], Aosheng Jiang[1], Yu Luo[1], Hongmei Cai[2], Guangda Ding[1], Philip White[1], Yu Liu[3], Xu Dong[4], Fangsen XU[1], Sheliang Wang[1], and Lei Shi[1]

[1]National Key Laboratory of Crop Genetic Improvement
[2]Huazhong Agricultural University College of Resources and Environment
[3]Zhejiang University College of Life Sciences
[4]Chinese Academy of Sciences State Key Laboratory of Magnetic Resonance and Atomic and Molecular Physics

April 20, 2022

Abstract

Recent progress has shown that vacuolar Pi transporters (VPTs) are important for cellular Pi homeostasis against external Pi variations in Arabidopsis and rice, while it is poorly understood for the identity and regulatory mechanism of VPTs in *Brassica napus* (*B. napus*). Here, we identified two vacuolar Pi influx transporters BnA09PHT5;1b and BnCnPHT5;1b in *B. napus* and uncovered their necessity for cellular Pi homeostasis through functional analysis. BnPHT5;1bs are the homologs of Arabidopsis AtPHT5;1 with the similar sequence, structure, tonoplast localization, and VPT activity. *BnPHT5;1b* double mutants had smaller shoot growth and higher shoot cellular Pi than the wild-type *B. napus*, which are largely different from the report in At *PHT5;1* mutant, suggesting PHT5;1-VPTs play a distinct mechanism of cellular Pi homeostasis in seedlings of *B. napus* and *Arabidopsis*. By contrast, disruption of *BnPHT5;1b* genes slowed vegetative growth accompanied by Pi toxicity in floral organs, reduced seed yield and impacted seed traits, agreeing with the role of AtPHT5;1 in floral Pi homeostasis. Taken together, our studies identified two vacuolar Pi influx transporters in *B. napus* and revealed the distinct and conserved regulatory mechanisms of BnPHT5;1bs in cellular Pi homeostasis in this plant species.

Introduction

Phosphorus (P) is an essential component of many macromolecules such as nucleic acid, phospholipid and ATP and plays vital roles in numerous metabolism pathways and signal transduction (White and Hammond 2008). Although high amounts of P exist in soil, the low availability of phosphate (Pi) is a key challenge for crop production due to its easily high fixation in soils. Phosphorus (P) deficiency unbalances plant cellular Pi homeostasis, a primary determinant of plant growth (Veneklaas et al., 2012). To adapt to P limitation, plants have evolved several mechanisms to fine-tune cellular Pi homeostasis. For example, under Pi-limited conditions, organic acids and acid phosphatase exuded by plants can improve Pi availability (Joan et al. 2017; Wang et al. 2018; Yang et al. 2019, 2021; Deng et al., 2022). In addition, the core transcription factor PHOSPHATE STARVATION RESPONSE 1 (PHR1) is activated rapidly to up-regulate the high-affinity Pi transporters PHOSPHATE TRANSPORTER 1 (PHT1) (Chiou and Lin 2011). Subsequently, dephosphorylation of endoplasmic reticulum (ER)-localized PHT1 proteins facilitate their trafficking to the plasma membrane (González et al., 2005; Bayle et al., 2011; Chen et al., 2011). These processes are required to facilitate greater Pi acquisition from the environment.

Excess P supply disrupts cellular Pi homeostasis. The formation of SPX-PHR complexes down-regulates

1

PHT1 expression by preventing the PHRs from entering the nucleus and inhibiting promoter binding capability, leading to reduction of Pi influx from the environment (Lv et al., 2014; Zhong et al., 2018; Osorio et al., 2019; Ried et al., 2021). In parallel, the degradation of PHT1 protein ubiquitinated by NLA1 also contributes to cellular Pi homeostasis under excess P conditions (Lin et al., 2013; Park et al., 2014). AtPHO1 and its homologous gene PHO1;H1 function in loading Pi into the root xylem for transport to the shoot (Hamburger et al. 2002; Stefanovic et al. 2007). Excess Pi prevents Pi transportation from roots to shoots by initiating the PHO2/NLA1 mediated degradation of PHO1 (Lin et al., 2013; Huang et al., 2013; Yue et al., 2017). The PHO1 family members are SPX-EXS (SYG1/PHO81/XPR1- ERD1/XPR1/SYG1) proteins and NLA1 is an SPX-RING (Really Interesting New Gene) protein (Liu et al., 2018).

Besides the regulation of cellular Pi homeostasis through Pi acquisition from the environment and translocation from the roots to the shoots, the vacuole-localized SPX-MFS (Major Facility Superfamily) proteins (also known as PHT5 proteins), which mediate Pi transport into the vacuole, can also contribute to cellular Pi homeostasis. In higher plants, the vacuole is the major Pi reservoir (Veneklaas et al., 2012) and provides strong buffering capacity for cellular Pi dynamics because the ratio of vacuolar Pi/total Pi can be controlled over a large range of concentrations (Dietz et al., 1986). In rice, the SPX-MFS3 protein was initially proposed to be a Pi efflux transporter, as evidenced by the lower vacuolar Pi content in an overexpression line of SPX-MFS3 compared to wild-type rice (Wang et al., 2015), but this interpretation was recently challenged by another group (Xu et al., 2019), who found that rice overexpressing SPX-MFS3 had higher vacuolar Pi content and mutants lacking SPX-MFS3 had lower vacuolar Pi concentrations than that wild-type rice, suggesting that SPX-MFS3 encoded a vacuolar Pi influx transporter. The rice SPX-MFS1 was found to mediate vacuolar Pi influx when expressed in yeast (Wang et al., 2012). In Arabidopsis, PHT5;1/VPT1 was identified as a vacuolar Pi influx transporter (Liu et al., 2015; Liu et al., 2016). *VPT1* has the highest expression in root and young leaves, then mature leaves followed by old leaves and is strongly induced by high Pi conditions in roots, mature leaves and old leaves (Liu et al., 2015). Disruption of *VPT1* rendered plants phenotypically hypersensitive to variations in Pi supply accompanied with reduced cellular Pi contents and vacuolar Pi contents (Liu et al., 2015; Liu et al., 2016), suggesting that *VPT1* functions in Pi storage in vacuole under conditions of Pi sufficiency and excess. Two vacuolar Pi efflux transporters VPE1 and VPE2 were recently identified in rice and the *vpe1 vpe2* double mutants (DM) had higher vacuolar Pi concentrations than the wild-type rice (Xu et al., 2019). In particular, the adaptability of *vpe1 vpe2* double mutants to changing Pi availability was significantly reduced (Xu et al., 2019). These results indicate that both vacuolar Pi influx and efflux transporters are essential for cellular Pi homeostasis and plant growth.

Oilseed rape (*Brassica napus* L .) is a major oil crop with a complex genome. *Brassica napus* has high P demand and is sensitive to Pi fluctuations in the environment. Its vacuolar Pi influx/efflux transporters have not yet been identified and the mechanisms underling cellular Pi homeostasis by vacuole remain elusive. In this study, we identified eight *PHT5* (SPX-MFS) genes in *B. napus* and further investigated the role of two *BnPHT5;1b* genes in cellular P dynamics. The predicted BnPHT5;1b proteins located in the tonoplast and expression of *BnPHT5;1bs* complemented the Pi adaptability of Arabidopsis *pht5/vpt1* mutant. We further performed the Pi transport activity assay of BnPHT5;1b proteins in yeast and NMR spectroscopy analysis of vacuolar Pi concentrations between wild type*B. napus* cultivar Westar 10 (W10) and *BnPHT5;1b* double mutants (DM). The results indicated that BnPHT5;1b proteins function as Pi influx transporters for vacuolar Pi storage. Genetic disruption of two *BnPHT5;1b* genes significantly reduced the adaptability of*B. napus* seedlings to Pi supply accompanied by high shoot cellular Pi concentrations, which is different from the *pht5/vpt1*mutant seedlings. At the reproductive stage, disruption of*BnPHT5;1b* genes caused Pi toxicity in floral organs and reduced seed yields under Pi-sufficient and high Pi conditions. In addition,*BnPHT5;1b* DM had abnormal seed traits and higher seed P concentrations compared to W10. Our results highlight the importance of BnPHT5;1b proteins as vacuolar Pi influx transporters in cellular Pi homeostasis in *B. napus*.

Materials and methods

Plant Materials and Growth Conditions

The *B. napus* cultivar 'Westar 10' curated in our laboratory was used for phenotypic analyses and mRNA

expression profiling. Seeds were surface-sterilized for 12 minutes using 1% NaClO and washed five times with pure water. Then, the seeds were germinated on a piece of gauze moistened with pure water. After 7 days, uniformly sized seedlings were transferred to one-half strength Hoagland nutrient solution refreshed every four days. The normal concentration of KH_2PO_4 in Hoagland nutrient solution (Hoagland and Arnon, 1950) was 100 μM unless otherwise stated. Plants were cultivated in a growth room at 22 with a 16-h-light/8-h-dark photoperiod (with a photon flux density of 300-320 lmol m^{-2} s^{-1}). Arabidopsis seedings were grown for one week on solid 1/2 MS (Murashige and Skoog) medium (Murashige and Skoog, 1962) then transferred to ANS (Arabidopsis nutrition solution) (Liu et al., 2016). For pot experiment, 7 kg soil/ pot was soaked 2,000 ml water including 3.005 g KNO_3, 1.75 g $MgSO_4 \cdot 7H_2O$, 4.643 g $(NH_4)_2SO_4$ and 7 ml Arnon storage solution (1,000 $\times$), 7 ml $FeSO_4 \cdot EDTA$ Hogland storage solution (200 $\times$), 755.5 mg/kg or 2,518.3 mg/kg $NaH_2PO_4 \cdot 2H_2O$.

RNA isolation and qRT-PCR.

Total RNA was isolated using a Promega RNA isolation kit (Eastep® Super), then cDNA was synthesized using a CWBIO kit (CW0690L). The real-time quantitative PCR was performed by the quantitative fluorescence kit (SYBR® Premix Ex TaqTM II, Takara, Kyoto, Japan) using a Real-time PCR detection system in Bio-Rad's ICYCleriQS fluorescent quantitative PCR instrument. The nucleotide sequences of the primer pairs used for qRT-PCR and cloning are shown in Supplementary Table 1.

Plasmid construction and plant transformation

To develop *BnA09PHT5;1b* /*vpt1* and *BnCnPHT5;1b* /*vpt1* transgenic plants and the Arabidopsis *BnPHT5;1b* overexpressing plants, the full-length coding sequence of each *BnPHT5;1b* gene was amplified from 'Westar 10' then inserted into the PMDC83-GFP vector at the EcoRI and XbaI restriction sites driven by the CaMV35S promoter. To generate GUS reporter lines, the 1,300 bp promoters of *BnA09PHT5;1b* and *BnCnPHT5;1b* were amplified and introduced into the DX2181b-GUS plasmid using the In-Fusion HD Cloning kit (Takara Bio). Transgenic Arabidopsis were produced using the method of Clough and Bent (1998). To generate *BnPHT5;1b* double mutants, a pair of *BnPHT5;1b* target sequences sgRNA1 (CGTGAT-ACAGAGGAACAAGA) and sgRNA2 (TGTTCCTCTGTATCACGCAG) were designed using CRISPR-P (http://crispr.hzau.edu.cn/CRISPR2/). Then the pKSE401 vector (Xing et al., 2014) was used to generate the Cas9-*BnPHT5;1b* construct, which used the AtU6-26 and AtU6-29 promoters to drive two sgRNAs expressions respectively. Transformation of *B. napus* was performed using the hypocotyl of Westar 10 for Agrobacterium infiltrating (De Block et al., 1989).

Histochemical localization of GUS expression

GUS histochemical staining was performed using a GUS staining kit (SL7160,Coolaber). The *ProBnA09PHT5;1b:GUS* and *ProBnCnPHT5;1b:GUS* transgenic plants were grown in a standard 1/2 MS nutrient solution for 5 days and then transferred to 100 μM and 1,000 μM Pi conditions for 5 days. The whole plants submerged in GUS staining solution were incubated in the dark at 37 for 8 hrs. After staining, the tissues were washed with 75% ethanol to remove chlorophyll and imaged by microscope (SMZ25,Nikon).

Subcellular localization

For transient expression analysis in Arabidopsis protoplasts, the full-length coding sequence of each *Bn-PHT5;1b* gene was amplified from 'Westar 10' genome and then cloned into the PM999 vector driven by the CaMV35S promoter using the In-Fusion HD Cloning kit (Takara Bio). Transformation of Arabidopsis mesophyll protoplasts was performed with the method of Yoo et al. (2007). After 12-16 hrs incubation, the transformed protoplasts were treated with pure water to release vacuoles for GFP signal imaging (TCS SP8, Leica). For subcellular localization in tobacco (*Nicotiana benthamiana*), full-length coding sequences of each *BnPHT5;1b* gene was cloned into the PMDC83 vector driven by the CaMV35S promoter. The Agrobacterium GV3101 strain containing 35S:*BnPHT5;1b* :GFP was co-injected into 4-week-old tobacco leaves with a mCherry labeled tonoplast marker (*A$\tau\gamma$TIII* :mCherry) and plasma membrane marker (*At-PIP2;:* mCherry), respectively. After 2 days, the fluorescence signals were examined using laser confocal

3

fluorescence microscopy (STELLARIS, Leica).

Pi transport activity assay in yeast

To generate vectors for yeast expression, the VPT1 and BnPHT5;1b coding regions were amplified from Col-0 and 'Westar 10' and cloned into the PRS426–ADH1 vector by the In-Fusion HD Cloning kit (PT5162-1, Takara Bio). The PRS426–ADH1-PHO84 and PRS426–ADH1- PHO91 vectors were provided (Xu et al. 2019). These constructs and empty vector were transformed independently into the yeast strain YP100. Yeast was grown in SD/-Trp-Ura media with 0.67% yeast nitrogen base, 2% galactose, 0.2% -Trp-Ura amino acids, 1.5% agar at pH 5.6 and incubated at 30 °C for 3 days. Colonies were picked for further growth in SD/- Trp-Ura liquid media until they reached an OD600 of 0.1. The strains were collected and washed twice with sterile water and then diluted 10-, 100-, 1000-fold with ddH$_2$O. Yeasts containing 5 μL diluted solution was spotted on SD (YNB-Pi) /-Trp-Ura media plates supplemented with 2% glucose, 30 mM KH$_2$PO$_4$ at 30 °C for survival test.

Measurement of Pi concentrations and total P concentration

The Pi concentration was measured using the method described previously by Lu et al. (2016). 50 mg of fresh tissue was harvested and mixed with 50 μL of 5 M H$_2$SO$_4$, then 1.5 mL pure water was added to each sample after grinding. The mixture was centrifuged at 12,000 g for 10 min at 4°C. The supernatant was collected and diluted to an appropriate concentration. The diluted supernatant was reacted with a malachite green reagent (19.4 mM H$_3$BO$_3$, 27.64 mM (NH$_4$)$_6$MO$_7$O$_{24}$·4H$_2$O, 2.38 M H$_2$SO$_4$, 627.5 μM malachite green, and 0.1% polyvinyl alcohol) in a 3:1 ratio for 30 min. 200 μl reaction mixture was taken to measure the absorption values at 650 nm by an ELIASA (Spark, TECAN). A standard curve was established using varying concentrations of KH$_2$PO$_4$ for the calculation of sample Pi concentrations. For measurement of total P concentration, 150 mg of dried plant tissue was pre-digested overnight in glass tubes with concentrated sulfuric acid. The tubes were then heated to 120 °C with 4–5 drops of 30% H$_2$O$_2$ every 30 min until the solution turned colorless. After 30 min extension of heat digestion, the total P concentration was determined by molybdenum blue colorimetry at 700 nm by an ELIASA (Spark, TECAN).

Measurement of anthocyanin conentration

Anthocyanins were extracted using the method of Lotkowska et al. (2015). About 0.1g fresh sample of rapeseed leaves was homogenated in 1mL of anthocyanin extract buffer (1% v/HCl, 99% v/n-propanol), followed by incubation at 98°C for 3 min. After 10˜12 hrs further incubation in the dark at room temperature, the mixture was centrifuged at 12,000 rpm for 10 min. 200 μL aliquots of the supernatant were measured absorbance at 535 nm and 650 nm by ELIASA (Spark, TECAN). Extraction buffer served as blank control.

^{31}P NMR analysis of vacuolar Pi.

The method was slightly modified from that of Xu et al. (2019). Approximately 0.05 g *B. napus* roots were used for NMR analysis. The roots were packed into a 5-mm-diameter NMR tube equipped with a perfusion system (5 mM glucose, 10 mM KNO$_3$, 0.5 mM Ca(NO$_3$)$_2$, 1 mM KCl, 0.5 mM MgSO$_4$, 100 μM KH$_2$PO$_4$, 2 mM MES, pH 5.5) connected to a peristaltic pump.^{31}P-NMR spectra were recorded using a standard broadband 5-mm probe on a Bruker Ascend 500 spectrometer with TopSpin software v.3.0. The ^{31}P-NMR spectra were recorded at 242.9 MHz lock with deuteroxide in two 0.5-mm glass capillaries. The^{31}P-NMR acquisition conditions were set as follows: 30° radiofrequency pulses (70 μs) at 2 s relaxation delay; 24 KHz spectral width; Waltz-based broadband proton decoupling (44 W during acquisition time, 0.6 W during delay) with a probe temperature of 25 °C. Free induction decays (FIDs) were collected as 16 K data points, zero-filled to 32 K, and processed with a 30-Hz exponential line broadening. Each spectrum was acquired over 0.34 s and was the sum of 3,600 scans. Other conditions followed the description by Xu et al. (2019).

Results

Identification and expression analysis of *PHT5* genes to P dynamics in *B. napus*

To identify the *PHT5* genes in *B. napus* , we performed a BLAST search in *B. napus* cultivar 'Darmor-*bzh* ' genome (Chalhoub et al., 2014) using the *AtPHT5;1* , *AtPHT5;2* and *AtPHT5;3* gene sequences. A total of eight close homologs of *AtPHT5* were identified, namely *BnA09PHT5;1a* , *BnC09PHT5;1a* , *BnA09PHT5;1b* , *BnCnPHT5;1b* , *BnA09PHT5;2* , *BnC09PHT5;2* , *BnA01PHT5;3* and *BnC01PHT5;3* (Figure 1a). Gene structure analysis showed that these BnPHT5 genes had 9 or 10 exons, encoding comparable length proteins (Figure S1, 695-705 amino acid residues). Based on protein sequence alignment, eight members of *BnPHT5* family showed more than 90% protein identities between the homologs of Arabidopsis and *B. napus* (Table 1).

To estimate the response of the *BnPHT5* genes to P supply, quantitative RT-PCR (qRT-PCR) was performed on 3-week-old *B. napus* leaves grown with different external Pi supply (0-100 μM). Both *BnPHT5;1a* and *BnPHT5;3* genes had the highest expression at 0 μM Pi supply and significantly declined at the 5-100 μM Pi supply (Figure 1a, d, e, g). In contrast, *BnA09PHT5;1b* and *BnCnPHT5;1b* were gradually induced as Pi supply increased (Figure 1c, f). These results suggest that *BnPHT5;1b* genes might play a different role from the *BnPHT5;1a* and *BnPHT5;3* genes in the *B. napus* Pi response. The expression of *BnA09PHT5;2* and *BnC09PHT5;2* could not be detected in our experimental conditions (data not shown).

Expression pattern of *BnPHT5;1b* genes

We further focused on the expression pattern of *BnPHT5;1b* genes in *B. napus* . To this end, the expression levels of *BnA09PHT5;1b* and *BnCnPHT5;1b* genes in the leaves and roots at 5 μM, 100 μM and 1000 μM Pi supply were measured (Figure 2a). Expression of *BnA09PHT5;1b* and *BnCnPHT5;1b* was greater in leaves than in roots (Figure 2a). *BnA09PHT5;1b* was induced by Pi supply in all tissues except in young leaves at 5 μM and 100 μM Pi supply (Figure 2a). The expression of *BnCnPHT5;1b* in roots was higher at 100 μM and 1,000 μM Pi supply than that of 5 μM Pi supply, and that in the old and mature leaves was similar between at 5 μM and 100 μM Pi supply but increased greatly at 1,000 μM Pi supply (Figure 2a). Interestingly, downregulation of *BnCnPHT5;1b* in young leaves was observed at 100 μM Pi supply compared with 5 μM and 1,000 μM Pi supply (Figure 2a). To understand the details of tissue expression, we established transgenic Arabidopsis lines expressing $\Pi\rho o B\nu A09\Pi HT5\cdot1\beta$: β-$\gamma\lambda\upsilon\varsigma\upsilon\rho o\nu\iota\delta\alpha\sigma\epsilon$ (*GUS*) and *ProBnCnPHT5;1b: GUS* , respectively. GUS staining results indicated that *BnA09PHT5;1b* and *BnCnPHT5;1b* have similar tissue expression patterns with evident transcriptional activity in root vascular bundle and leaf vein (Figure 2b, c). These results suggest that *BnPHT5;1b* genes may be involved in cellular Pi homeostasis in multiple tissues.

BnPHT5;1bs **functionally complement *Atpht5;1* growth defects**

The high protein sequence identities of BnA09PHT5;1b and BnCnPHT5;1b and AtVPT1/AtPHT5;1 (Figure S2) imply that BnPHT5;1b proteins might have a tonoplast localization and Pi transport activity. A novel neural network-based model, Alphafold provides accurate protein 3-D structure prediction (Jumper et al., 2021). Alphafold was used to predict the 3-D structure of BnPHT5;1b proteins and to compare them with AtVPT1. As expected, both BnA09PHT5;1b or BnCnPHT5;1b showed a high degree of coincidence in 3-D structure with the AtVPT1 protein, especially in the domains composed of helices (Figure 3a, b). To validate the localization of BnA09PHT5;1b and BnCnPHT5;1b, green fluorescent protein (GFP) labeled BnA09PHT5;1b and BnCnPHT5;1b were constructed and their subcellular localization was analyzed in Arabidopsis protoplast. As shown in figure 3C, the GFP signals were observed on the tonoplast, indicating that BnA09PHT5;1b and BnCnPHT5;1b localized on the vacuole membrane. Such tonoplast localization of BnA09PHT5;1b and BnCnPHT5;1b proteins were further confirmed when 35s:GFP-BnA09PHT5;1b or 35s:GFP-BnCnPHT5;1b were co-expressed in tobacco (*Nicotiana benthamiana*) leaves with γTIP:mCherry, a tonoplast marker (Figure S3).

To analyze the Pi transport activity of these two BnPHT5;1 proteins, a yeast mutant (YP100) was employed. The YP100 yeast mutant lacks the function of Pi transport, thus cannot survive (Popova et al., 2010). When induced in YP100 yeast, PHO84 (high-affinity Pi transporter) strain had much better growth than the PHO91 strain (low-affinity Pi transporter), suggesting that this yeast system can be used to assay Pi

5

transport activity. The AtVPT1 strain, BnA09PHT5;1b strain and BnCnPHT5;1b strain had comparable growth at 30 mM Pi supply (Figure 3d), suggesting that BnPHT5;1b proteins and AtVPT1 protein may have similar Pi transport activity in yeast.

Homozygous lines of 35s:BnA09PHT5;1b-GFP/*Atvpt1* and 35s:BnCnPHT5;1b/*Atvpt1* were generated by Agrobacterium-mediated transformation of *Arabidopsis thaliana* (Clough and Bent, 1998). Col-0, *Atvpt1* mutant and *BnPHT5;1b* transgenic lines were grown in Arabidopis nutrient solution (ANS solution) (Liu et al., 2016) for four weeks for phenotype comparison. The *Atvpt1* mutant developed shorter roots and smaller shoots than Col-0 plants from 13 μM to 3,900 μM Pi supply (Figure 4a, Figure S4). However, both*BnA09PHT5;1b* and *BnCnPHT5;1b* transgenic lines complemented the *Atvpt1* growth defects at all Pi supplies though the plants were slightly smaller than the Col-0 wildtype (Figure 4a, b). Phosphorus concentrations were elevated in all *BnPHT5;1b* transgenic plants compared to the *Atvpt1* mutant (Figure 4c). These results demonstrate that *BnPHT5;1b* genes can functionally complement the*Atvpt1* growth defects. Moreover, overexpression of*BnPHT5;1b* genes individually in Col-0 background enhanced plant adaptability to fluctuations in Pi supply (Figure S5).

Vacuolar Pi influx is reduced in *BnPHT5;1b* double mutants

It can be argued that vacuolar Pi concentrations would be decreased in*BnPHT5;1b* loss-of-function mutants if they mediate vacuolar Pi influx. To avoid the effects of functional redundancy of homologous genes, we constructed *BnPHT5;1b* double mutants (DM) using a CRISPR-Cas9 based gene-editing system (Figure 5a). We then used Nuclear Magnetic Resonance (NMR) spectroscopy to compare the root vacuolar Pi concentrations in the DM plants and the wild-type W10 plants. Plants grown in 100 μM Pi conditions were transferred to 1,000 μM Pi supply for 2 hours before NMR analysis. The vacuolar Pi concentration in W10 was 17.85 $\pm$ 2.3 mmol Pi g^{-1} FW, while it was significantly less in the vacuoles of DM plants (8.41 $\pm$ 1.7 mmol Pi g^{-1} FW) (Figure 5b, c). This result demonstrates that BnPHT5;1b proteins mediate vacuolar Pi influx.

BnPHT5;1b **genes are required for the adaptability of***B. napus* **to fluctuations in Pi supply**

To investigate the role of *BnPHT5;1b* genes in the cellular Pi homeostasis in *B. napus* , the P response for *BnPHT5;1b* DM plants and W10 plants were compared phenotypically. 10-day-old plants grown with 100 μM Pi supply in a hydroponic system were transferred to 100 μM or 1,000 μM Pi supply for 7 days.*BnPHT5;1b* DM plants had lower shoot fresh weight than W10 at both Pi supplies and the fresh weight of the root was slightly less in *BnPHT5;1b* DM plants compared to W10 at both Pi supplies (Figure 6a, b), leading to increased root-shoot ratios of *BnPHT5;1b* DM plants, especially at high Pi supply (Figure 6c). Notably, the difference in shoot fresh weight between W10 and *BnPHT5;1b* DM plants was greater in 1,000 μM Pi supply (fresh weight 64% - 71% relative to W10) than in 100 μM Pi supply (fresh weight 59% - 66% relative to W10) (Figure 6b). Interestingly, the Pi concentrations were greater in shoots and lower in roots of *BnPHT5;1b* DM plants than in W10 at both Pi supplies (Figure 6d), while the percentage of Pi increase after 1,000 μM Pi treatment was lower in all leaves but rather in the roots of*BnPHT5;1b* DM plants compared to W10 (Figure 6e). This result suggests that loss-of-function of *BnPHT5;1b* genes reduce the Pi storage capacity in leaves of *BnPHT5;1b* DM plants grown with a sufficient Pi supply.

It is reasonable to assume that reduced vacuolar Pi storage capacity rendered weak buffering capacity to Pi deficiency stress. To test this, five -day-old plants (W10 and DM) grown with 100 μM, 1,000 μM and 2,000 μM Pi supply were transferred to a solution lacking Pi for 14 days of growth. As expected, Pi deprivation dramatically inhibited plant growth, of which the biggest difference in biomass between DM plants and W10 plants was observed in plants grown initially with 2,000 μM Pi supply (40.3%-55.2%) compared with plants grown initially with 1,000 μM Pi supply (29.3%-37.5%) and 100 μM Pi supply (29.0%-37.4%) (Figure 7a, b). Interestingly, leaves of *BnPHT5;1b* DM plants still had significantly greater Pi concentrations than W10 plants grown initially with 1,000 μM and 2,000 μM Pi supply (Figure 7c). Consistently, the leaves of the *BnPHT5;1b* DM plants had significantly higher anthocyanin contents than W10 plants grown initially with 1,000 μM and 2,000 μM Pi supplies, suggesting that the larger Pi concentrations caused more acute

6

Pi stress in leaves of *BnPHT5;1b* DM plants than in W10 plants (Figure 7d). Nevertheless, loss-of-function in*BnPHT5;1b* genes disrupted cellular Pi homeostasis, which reduced the adaptability of *B.napus* seedlings to fluctuations in Pi supply.

BnPHT5;1b genes are required for reproductive growth and seed traits

Both *BnA09PHT5;1b* or *BnCnPHT5;1b* had strong expression in mature leaves, young leaves and flowers at the reproductive stage (Figure 8a). To evaluate the influence of *BnPHT5;1s* on reproductive growth, W10 and two *BnPHT5;1b* DM lines were grown in pots with soil supplemented with 150 mg P/kg soil (normal P supply; NP) and 500 mg P/kg soil (high P supply; HP), respectively (Figure S6 a, b). Under NP conditions, *BnPHT5;1b* DM plants had shorter stems (plant height) and smaller dry weight than W10 plants, while high P supply improved the growth of *BnPHT5;1* DM plants to approximate W10 plants in plant height but not in dry weight (Figure S6c). The total P concentration in stem, leaves and flowers showed that *BnPHT5;1* DM plants had larger total P concentration in flowers than in W10 in NP conditions (Figure 8b) and also larger Pi concentrations in the stamen, pistil, petal and sepal (Figure 8c). Under HP conditions,*BnPHT5;1b* DM plants had larger total P concentration in their flowers while W10 plants had larger total P concentration in the stem (Figure 8d). Therefore, *BnPHT5;1b* DM plants had distributed more total P to flowers than W10 plants under both NP and HP conditions (Figure S6c, d). A previous study reported that an Arabidopsis mutant lacking vacuolar Pi influx transporter, *Atvpt1 Atvpt3* , showed Pi toxicity in floral organs when grown under Pi-sufficient conditions, leading to the inhibition of pollen tube growth and reproductive impairment (Luan et al., 2019). We therefore compared traits related to seed yield between W10 and *BnPHT5;1b* DM plants. Although there were no significant differences of branch numbers between*BnPHT5;1b* DM plants and W10 plants under NP or HP conditions (Figure S7a, b, d), a decrease in silique numbers and seed yield per plant was observed in *BnPHT5;1b* DM plants compared to W10 plants under both NP and HP conditions (Figure 8e, f). Therefore, the reduction in seed yield in *BnPHT5;1b* DM plants could be ascribed to the excessive P/Pi accumulation in floral organs.

Furthermore, we found that seeds from *BnPHT5;1b* DM plants developed an irregular shape with a concave and convex surface, which differs from the approximately spherical shape of W10 seeds (Figure 9a). The diameter of seeds from *BnPHT5;1b* DM plants was larger than seeds from W10 plants (Figure 9b), indicating *BnPHT5;1b* DM had a larger seed size than W10. Indeed, the 1,000-grain weight of*BnPHT5;1b* DM seeds was also greater than W10 seeds (Figure 9c). In line with the high P/Pi concentrations in *BnPHT5;1b* DM flowers (Figure 8b, d), the P concentrations of *BnPHT5;1b* DM seeds were consistently greater than W10 seeds under both NP and HP conditions (Figure. 9d). However, the germination ratio of seeds from W10 plants was 97.0 ± 3.0%, while the germination ratio of seeds from*BnPHT5;1b* DM plants was only 73.0 ± 2.3% and 66.0 ± 3.0% (Figure 9e). These results indicate that *BnPHT5;1b* genes are required for reproductive growth, seed yield and seed yield related traits in *B. napus* .

Discussion

BnPHT5;1b proteins function as vacuolar Pi influx transporters

The phytoavailable form of P is Pi, but soil Pi concentrations often cannot satisfy crop growth requirements (Schachtman et al., 1998). The application of large amounts of Pi-containing fertilizers by farmers is a common agronomic practice to attain maximum agronomic production. It also causes large fluctuations in soil Pi concentration, requiring plants to adapt rapidly cellular Pi fluxes to maintain cellular Pi homeostasis. The importance of the regulation of Pi transporters in adjusting Pi uptake and delivery to the xylem in plant Pi homeostasishas been established (Wang et al., 2021). However, cellular Pi homeostasis cannot be achieved without utilizing the buffering capacity of the Pi major reservoirin plants, the vacuole (Veneklaas et al., 2012; Dietz and Foyer, 1986). Vacuolar Pi influx and efflux rely on the Pi influx and efflux transporters on the tonoplast, such as SPX-MFS3 in rice (Wang et al., 2015; Xu et al., 2019) and PHT5;1/VPT1 and PHT5;3/VPT3 in Arabidopsis (Liu et al., 2015; Liu et al., 2016; Luan et al., 2019).

Brassica napus is an allotetraploid oil crop with a more complex genome (AACC, 2n = 38) than the genomes of rice and Arabidopsis and is highly sensitive to Pi stress. The vacuolar Pi transporters and their roles in

7

cellular Pi homeostasis remain elusive. Based on the protein sequences of the AtPHT5 family, we identified 8 homologs in *B. napus* showing more than 90% amino acid sequence identities with AtPHT5 proteins (Figure 1a, Table 1). The BnA09PHT5;1a, BnC09PHT5;1a, BnA09PHt5;1b and BnCnPHT5;1b proteins were the homolog of AtPHT5;1 in *B. napus* (Figure 1a), however only the two *BnPHT5;1b* genes showed Pi induced expression pattern (Figure 1c, f and Figure 2), similar to the expression pattern of *AtPHT5;1* (Liu et al., 2015). The predicted 3-D structures of BnPHT5;1b and AtPHT5;1 had high similarity (Figure 3a, b). We thus hypothesized that BnPHT5;1b proteins may function as the vacuolar Pi influx transporters in *B. napus* . The BnPHT5;1b proteins were localized on the tonoplast and showed a comparable Pi transport activity to AtVPT1 when expressed in a yeast mutant (Figure 3c, d, Figure S3). Furthermore, vacuolar Pi concentration was smaller in *BnPHT5;1b* DM plants than wildtype W10 plants and both *BnPHT5;1b* genes could significantly recover the growth defects and P concentrations of the Arabidopsis *Atvpt1* mutant under various Pi conditions (Figure 4). Therefore, we conclude that BnPHT5;1b proteins function as vacuolar Pi influx transporters in *B. napus* .

PHT5;1-VPTs play distinct regulatory mechanisms of cellular Pi homeostasis between *B. napus* seedlings and *Arabidopsis* seedlings

In *Arabidopsis thaliana* , the *PHT5* family includes 3 members (*PHT5;1* , *PHT5;2* and *PHT5;3*) and *PHT5;1* plays a predominant role in cellular Pi homeostasis (Liu et al., 2015, 2016). *PHT5;1* is expressed mainly in roots and young leaves and its expression is increased by increasing Pi supply in roots, mature and old leaves (Liu et al., 2015). Consistent with the response of *AtPHT5;1* to Pi supply, both *BnA09PHT5;1b* and *BnCnPHT5;1b* were strongly induced by high Pi supply in roots and older leaves when plants were transferred from 5 μM Pi to 100 μM Pi supply and in all tissues when transferred to 1,000 μM Pi supply (Figure 2). Slower growth than wild-type plants was observed in the roots and shoots of *Atpht5;1* mutant at Pi concentrations from 13 μM to 6.5 mM (Liu et al., 2015), while only in the shoots of *BnPHT5;1b* DM plants at Pi concentrations 100 and 1,000 μM (Figure 6). These results suggested that AtPHT5;1 functions in both roots and shoots, but BnPHT5;1b affect primarily shoot growth.

Differences in fresh weights of shoots were always greater than differences in fresh weights of roots between W10 and *BnPHT5;1b* DM plants when grown under both Pi-sufficient conditions (100 μM) and high Pi conditions (1,000 μM) (Figure 6 and Figure 7). Consistently, *BnPH5;1b* DM plants had increased root-to-shoot ratios compared with W10 (Figure 6c). Notably, the *BnPHT5;1b* DM plants had greater Pi concentrations in shoots than W10 when grown under both Pi-sufficient and high Pi conditions (Figure 6d). Given that *BnPHT5;1bs* had strong expression in root vascular tissue (Figure 2b, c), dead cells of xylem are not the target of *BnPHT5;1b* . Disruption of *BnPHT5;1bs* function might not have interference on the long-distance transport of Pi from roots to shoots. Because vacuolar Pi was lower in *BnPHT5;1b* DM plants than in W10, thus the higher Pi concentrations in the shoot of *BnPHT5;1b* DM plants can only be the consequence of cytoplasmic Pi accumulation. The elevated cytoplasmic Pi level is harmful to shoot growth. In contrast, *Atpht5;1/vpt1* mutant has lower shoot Pi content and cytosolic Pi level than the wild-type (Liu et al., 2016, Luan et al., 2019). ProAtPHT5;1:GUS showed strong expression of non-vascular cells, which may provide an interpretation that loss-of-function in *AtPHT5;1* severely hinders root growth (Liu et al., 2015).

VPE1 and VPE2 are the vacuolar Pi efflux transporters and direct vacuole-to-cytosol Pi movement for Pi remobilization under Pi-deprived conditions (Xu et al., 2019). We proposed that reduced vacuole storage of Pi in *BnPHT5;1b* DM plants would render plants sensitive to Pi-deficient conditions. *Brassica napus* seedlings grown for 5 days with 100 μM, 1,000 μM and 2,000 μM Pi supplies, were subjected to 14 days of Pi deprivation. The slower growth of *BnPHT5;1* DM plants than W10 plants (Figure 7a, b) hardly be attributed to the decreased ability of vacuolar Pi remobilization because the Pi concentrations constantly higher in the shoots of *BnPHT5;1b* DM plants than the W10 plants (Figure 7c), indicating that *BnPHT5;1* DM plants had lower Pi reuse efficiency than W10 under Pi deprivation condition. Nonetheless, these results suggest that PHT5;1s play distinct regulatory mechanisms of cellular Pi homeostasis between *B. napus* seedlings and Arabidopsis seedlings.

PHT5;1-VPTs play a conserved role in floral Pi homeostasis between *B. napus* and *Arabidopsis*

.

In the Arabidopsis *pht5;1/vpt1* mutant, the absence of *PHT5;3* further reduced seedling Pi concentration, and vacuolar and cytosolic Pi concentrations when grown under Pi-sufficient conditions (Luan et al., 2019). In particular, the *pht5;1 pht5;3 (vpt1 vpt3)* double mutant rather than *pht5;1 /vpt1* single mutant showed Pi toxicity in floral organs and reproductive defects (Luan et al., 2019). This result agrees with our findings that *BnPHT5;1b* DM plants had larger floral Pi concentrations than W10 plants when grown under Pi-sufficient conditions (Figure 8c) and also displayed reproductive defects when grown under both Pi-sufficient and high Pi conditions in pots (Figure 8f). It was previously shown that Pi-toxicity has little effect on the morphology of floral organs but inhibits pollen tube growth as a consequence of excessive Pi concentration in the pistil (Luan et al., 2019). The *BnPHT5;1b* genes had strong expression in leaves and flowers (Figure 8a). Loss-of-function of *BnPHT5;1b* reduced Pi storage in leaves and lead to excessive Pi concentrations in flowers of plants grown under Pi-sufficient conditions (Figure S6c, d). Therefore, the excessive Pi concentration in the pistil of *BnPHT5;1b* DM plants was correlated with the reduction in seed yield. These results suggest that PHT5;1s play a conserved role in floral Pi homeostasis between *B. napus* and *Arabidopsis.*

In addition, the *BnPHT5;1b* DM seeds had abnormal phenotypes, particularly a larger P concentration than W10 seeds (Figure 9), suggesting that *BnPHT5;1b* genes might also play a crucial role in seed development. Although the role of *BnPHT5;1b* genes in seed development and the interrelationship between *BnA09PHT5;1b* and *BnCnPHT5;1b* in cellular Pi homeostasis needed further investigation, our findings demonstrate that BnPHT5;1b proteins play an essential role in cellular Pi homeostasis throughout the plant.

Acknowledgements

Author contributions

LS, SW, BH and CW contributed ideas. LS, SW, BH and CW designed experiments and interpreted results. BH performed all the experiments. TW, JY, AJ, YL, YL and XD helped with the experiments and manuscript preparation. BH and JY prepared the figures. LS, SW and BH wrote the manuscript. PJW, HC, GD and FX edited the manuscript.

Conflict of interest

Conflicts of interest: No conflicts of interest declared.

References

Bayle, V., Arrighi, J. F., Creff, A., Nespoulous, C., Vialaret, J., Rossignol, M., Gonzalez, E., Paz-Ares, J., and Nussaume, L. (2011). Arabidopsis thaliana high-affinity phosphate transporters exhibit multiple levels of posttranslational regulation. *Plant Cell* 23:1523–1535.

Chalhoub, B., Denoeud, F., Liu, S., Parkin, I. A. P., Tang, H., Wang, X., Chiquet, J., Belcram, H., Tong, C., Samans, B., et al. (2014). Early allopolyploid evolution in the post-neolithic Brassica napus oilseed genome. *Science (80-.).* 345:950–953.

Chen, J., Liu, Y., Ni, J., Wang, Y., Bai, Y., Shi, J., Gan, J., Wu, Z., and Wu, P. (2011). OsPHF1 regulates the plasma membrane localization of low- and high-affinity inorganic phosphate transporters and determines inorganic phosphate uptake and translocation in rice. *Plant Physiol.* 157:269–278.

Chiou, T.-J., and Lin, S.-I. (2011). Signaling Network in Sensing Phosphate Availability in Plants. *Annu. Rev. Plant Biol.* 62:185–206.

Clough, S. J., and Bent, A. F. (1998). Floral dip: A simplified method for Agrobacterium-mediated transformation of Arabidopsis thaliana.*Plant J.* 16:735–743.

De Block, M., De Brouwer, D., and Tenning, P. (1989). Transformation of Brassica napus and Brassica oleracea Using Agrobacterium tumefaciens and the Expression of the bar and neo Genes in the Transgenic Plants .*Plant Physiol.* 91:694–701.

Deng, S., Li, J., Du, Z., Wu, Z., Yang, J., Cai, H., Wu, G., Xu, F., Huang, Y., Wang, S., et al. (2022). Rice ACID PHOSPHATASE 1 regulates Pi stress adaptation by maintaining intracellular Pi homeostasis.*Plant Cell Environ.* 45:191–205.

Dietz, K. J., and Foyer, C. (1986). The relationship between phosphate status and photosynthesis in leaves - Reversibility of the effects of phosphate deficiency on photosynthesis. *Planta* 167:376–381.

González, E., Solano, R., Rubio, V., Leyva, A., and Paz-Ares, J. (2005). PHOSPHATE TRANSPORTER TRAFFIC FACILITATOR1 is a plant-specific SEC12-related protein that enables the endoplasmic reticulum exit of a high-affinity phosphate transporter in Arabidopsis. *Plant Cell*17:3500–3512.

Hamburger, D., Rezzonico, E., Petétot, J. M. D. C., Somerville, C., and Poirier, Y. (2002). Identification and characterization of the Arabidopsis PHO1 gene involved in phosphate loading to the xylem.*Plant Cell* 14:889–902.

Hawkins, H. J., Hettasch, H., Mesjasz-Przybylowicz, J., Przybylowicz, W., and Cramer, M. D. (2008). Phosphorus toxicity in the Proteaceae: A problem in post-agricultural lands. *Sci. Hortic. (Amsterdam)*.117:357–365.

Huang, T. K., Han, C. L., Lin, S. I., Chen, Y. J., Tsai, Y. C., Chen, Y. R., Chen, J. W., Lin, W. Y., Chen, P. M., Liu, T. Y., et al. (2013). Identification of downstream components of ubiquitin-conjugating enzyme PHOSPHATE2 by quantitative membrane proteomics in Arabidopsis roots.*Plant Cell* 25:4044–4060.

Joan, R., José Manuel, B. M., and Xavier, S. F. (2017). Phosphorus mobilization in low-P arable soils may involve soil organic C depletion.*Soil Biol. Biochem.* 113:250–259.

Jumper, J., Evans, R., Pritzel, A., Green, T., Figurnov, M., Ronneberger, O., Tunyasuvunakool, K., Bates, R., Žídek, A., Potapenko, A., et al. (2021). Highly accurate protein structure prediction with AlphaFold. *Nature* 596:583–589.

Lin, W. Y., Huang, T. K., and Chiou, T. J. (2013). NITROGEN LIMITATION ADAPTATION, a target of MicroRNA827, Mediates degradation of plasma membrane-localized phosphate transporters to maintain phosphate homeostasis in Arabidopsis. *Plant Cell* 25:4061–4074.

Liu, J., Fu, S., Yang, L., Luan, M., Zhao, F., Luan, S., and Lan, W. (2016). Vacuolar SPX-MFS transporters are essential for phosphate adaptation in plants. *Plant Signal. Behav.* 11:e1213474.

Liu, J., Yang, L., Luan, M., Wang, Y., Zhang, C., Zhang, B., Shi, J., Zhao, F. G., Lan, W., and Luan, S. (2015). A vacuolar phosphate transporter essential for phosphate homeostasis in Arabidopsis.*Proc. Natl. Acad. Sci. U. S. A.* 112:E6571–E6578.

Liu, N., Shang, W., Li, C., Jia, L., Wang, X., Xing, G., and Zheng, W. M. (2018). Evolution of the SPX gene family in plants and its role in the response mechanism to phosphorus stress. *Open Biol.* 8.

Liu, T. Y., Huang, T. K., Yang, S. Y., Hong, Y. T., Huang, S. M., Wang, F. N., Chiang, S. F., Tsai, S. Y., Lu, W. C., and Chiou, T. J. (2016). Identification of plant vacuolar transporters mediating phosphate storage. *Nat. Commun.* 7:1–11.

Lotkowska, M. E., Tohge, T., Fernie, A. R., Xue, G. P., Balazadeh, S., and Mueller-Roeber, B. (2015). The arabidopsis transcription factor MYB112 promotes anthocyanin formation during salinity and under high light stress. *Plant Physiol.* 169:1862–1880.

Lu, L., Qiu, W., Gao, W., Tyerman, S. D., Shou, H., and Wang, C. (2016). OsPAP10c, a novel secreted acid phosphatase in rice, plays an important role in the utilization of external organic phosphorus. *Plant Cell Environ.* 39:2247–2259.

Luan, M., Zhao, F., Han, X., Sun, G., Yang, Y., Liu, J., Shi, J., Fu, A., Lan, W., and Luan, S. (2019). Vacuolar phosphate transporters contribute to systemic phosphate homeostasis vital for reproductive development in arabidopsis 1[open]. *Plant Physiol.*179:640–655.

Lv, Q., Zhong, Y., Wang, Y., Wang, Z., Zhang, L., Shi, J., Wu, Z., Liu, Y., Mao, C., Yi, K., et al. (2014). SPX4 negatively regulates phosphate signaling and homeostasis through its interaction with PHR2 in rice.*Plant Cell* 26:1586–1597.

Osorio, M. B., Ng, S., Berkowitz, O., De Clercq, I., Mao, C., Shou, H., Whelan, J., and Jost, R. (2019). SPX4 Acts on PHR1-dependent and -independent regulation of shoot phosphorus status in arabidopsis.*Plant Physiol.* 181:332–352.

Park, B. S., Seo, J. S., and Chua, N. H. (2014). NITROGEN LIMITATION ADAPTATION Recruits PHOS-PHATE2 to target the phosphate transporter PT2 for degradation during the regulation of Arabidopsis phosphate homeostasis. *Plant Cell* 26:454–464.

Popova, Y., Thayumanavan, P., Lonati, E., Agrochão, M., and Thevelein, J. M. (2010). Transport and signaling through the phosphate-binding site of the yeast Pho84 phosphate transceptor. *Proc. Natl. Acad. Sci. U. S. A.* 107:2890–2895.

Ried, M. K., Wild, R., Zhu, J., Pipercevic, J., Sturm, K., Broger, L., Harmel, R. K., Abriata, L. A., Hothorn, L. A., Fiedler, D., et al. (2021). Inositol pyrophosphates promote the interaction of SPX domains with the coiled-coil motif of PHR transcription factors to regulate plant phosphate homeostasis. *Nat. Commun.* 12:1–13.

Schachtman, D. P., Reid, R. J., and Ayling, S. M. (1998). Phosphorus Uptake by Plants: From Soil to Cell. *Plant Physiol.* 116:447–453.

Stefanovic, A., Ribot, C., Rouached, H., Wang, Y., Chong, J., Belbahri, L., Delessert, S., and Poirier, Y. (2007). Members of the PHO1 gene family show limited functional redundancy in phosphate transfer to the shoot, and are regulated by phosphate deficiency via distinct pathways.*Plant J.* 50:982–994.

Veneklaas, E. J., Lambers, H., Bragg, J., Finnegan, P. M., Lovelock, C. E., Plaxton, W. C., Price, C. A., Scheible, W. R., Shane, M. W., White, P. J., et al. (2012). Opportunities for improving phosphorus-use efficiency in crop plants. *New Phytol.* 195:306–320.

Wang, C., Huang, W., Ying, Y., Li, S., Secco, D., Tyerman, S., Whelan, J., and Shou, H. (2012). Functional characterization of the rice SPX-MFS family reveals a key role of OsSPX-MFS1 in controlling phosphate homeostasis in leaves. *New Phytol.* 196:139–148.

Wang, C., Yue, W., Ying, Y., Wang, S., Secco, D., Liu, Y., Whelan, J., Tyerman, S., and Shou, H. (2015). OsSPX-MFS3, a vacuolar phosphate efflux transporter, is involved in maintaining Pi homeostasis in rice.*Plant Physiol.* Advance Access published 2015, doi:10.1104/pp.15.01005.

Wang, Y., Chen, X., Lu, C., Huang, B., and Shi, Y. (2017). Different mechanisms of organic and inorganic phosphorus release from mollisols induced by low molecular weight organic acids. *Can. J. Soil Sci.*98:15–23.

Wang, Z., Kuo, H. F., and Chiou, T. J. (2021). Intracellular phosphate sensing and regulation of phosphate transport systems in plants.*Plant Physiol.* 187:2043–2055.

White, P. J. , Hammond, J. P. (2008) Phosphorus nutrition of terrestrial plants. In: The Ecophysiology of Plant-Phosphorus Interactions, pp. 51-81. White PJ, Hammond JP, eds. Springer, Dordrecht. ISBN 978-1-4020-8434-8.

11

Xing, H. L., Dong, L., Wang, Z. P., Zhang, H. Y., Han, C. Y., Liu, B., Wang, X. C., and Chen, Q. J. (2014). A CRISPR/Cas9 toolkit for multiplex genome editing in plants. *BMC Plant Biol.* 14:1–12.

Xu, L., Zhao, H., Wan, R., Liu, Y., Xu, Z., Tian, W., Ruan, W., Wang, F., Deng, M., Wang, J., et al. (2019). Identification of vacuolar phosphate efflux transporters in land plants. *Nat. Plants* 5:84–94.

Yang, X., Chen, X., Guo, E., and Yang, X. (2019). Path analysis of phosphorus activation capacity as induced by low-molecular-weight organic acids in a black soil of Northeast China. *J. Soils Sediments* 19:840–847.

Yoo, S. D., Cho, Y. H., and Sheen, J. (2007). Arabidopsis mesophyll protoplasts: A versatile cell system for transient gene expression analysis. *Nat. Protoc.* 2:1565–1572.

Yue, W., Ying, Y., Wang, C., Zhao, Y., Dong, C., Whelan, J., and Shou, H. (2017). OsNLA1, a RING-type ubiquitin ligase, maintains phosphate homeostasis in Oryza sativa via degradation of phosphate transporters. *Plant J.* **90** :1040–1051.

Zhong, Y., Wang, Y., Guo, J., Zhu, X., Shi, J., He, Q., Liu, Y., Wu, Y., Zhang, L., Lv, Q., et al. (2018). Rice SPX6 negatively regulates the phosphate starvation response through suppression of the transcription factor PHR2. *New Phytol.* **219** :135–148.

**Table 1 The *PHT5* family members in *Brassica napus* and their common structural features**

| Arabidopsis genes	*Brassica napus* paralogs	Sequence annotation in *Brassica napus*	Genomic sequence length (bp)	Exons	Protein size (aa)	Conserved domain	Amino acid sequence identity with *AtPHT5* (%)	Amino acid sequence identity between Paralog (%)
AtPHT5;1	*BnA09PHT5;1*	*BnaA09g12960*	4000	9	698	SPX、MFS	90.6	98
	BnC09PHT5;1	*BnaC09g12880*	2914	9	695	SPX、MFS	90.6	
	BnA09PHT5;1b	*BnaA09g53000*	4550	10	703	SPX、MFS	90.9	99.4
	BnCnPHT5;1b	*BnaCnng51450*	4230	10	703	SPX、MFS	91.2	
AtPHT5;2	*BnA09 PHT5;2*	*BnaA09g21340*	2970	9	705	SPX、MFS	91.4	99.1
	BnC09PHT5;2	*BnaC09g23750*	2878	9	705	SPX、MFS	91.5	
AtPHT5;3	*BnA01PHT5;3*	*BnaA01g12800*	4020	10	701	SPX、MFS	90.6	97.6
	BnC01PHT5;3	*BnaC01g14580*	3014	10	696	SPX、MFS	90	

Figures:
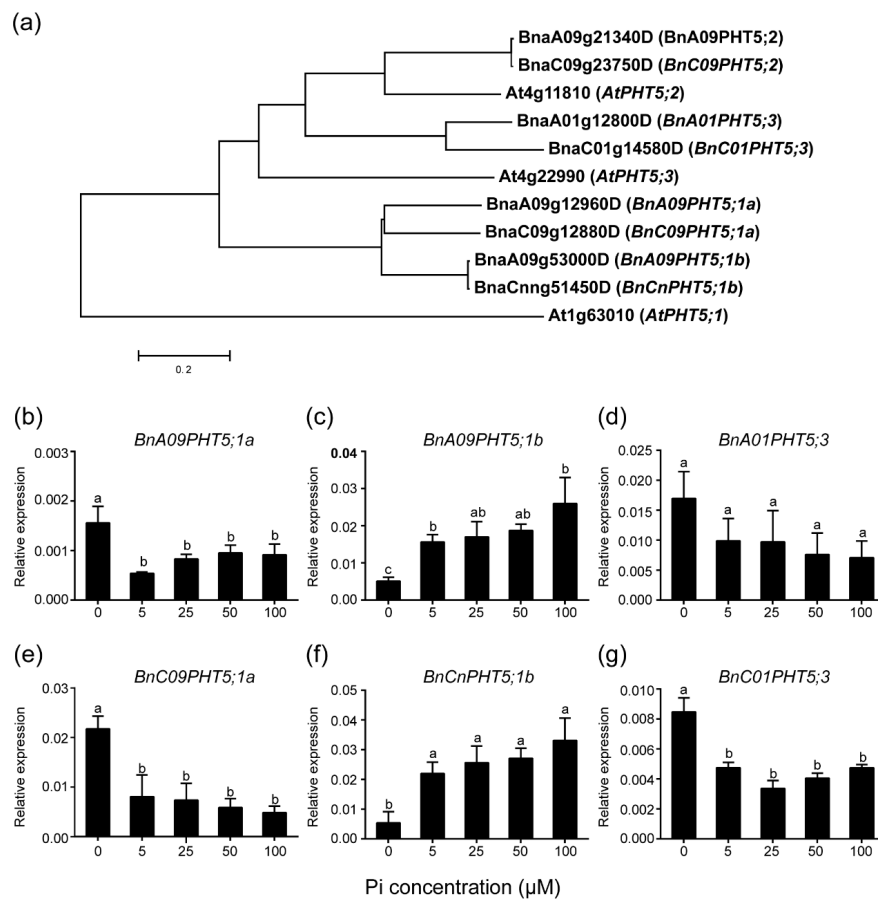
Figure 1. Identification of the PHT5 family of proteins in *Brassica napus* and their transcriptional response to Pi supply.

(a) The PHT5 family in *Brassica napus* and *Arabidopsis* . The phylogenetic tree was generated by MEGA 6 using the protein sequence of *AtPHT5* family members and BnPHT5 family members with the neighbor-joining (NJ) method and 1000 bootstrap replicates. **(b-g)** qRT-PCR analysis of the expression of the *BnPHT5* family in leaves grown at different phosphorus supplies. The relative expression level of *BnPHT5;1a* **(b, e)** , *BnPHT5;1b* **(c, f)** and BnPHT5;3 **(d, g**) in *Brassica napus* cultivar Westar 10 grown with different phosphorus concentrations in a hydroponic medium (0 μM, 5 μM, 25 μM, 50 μM and 100 μM P supply). 9-day-old *Brassica napus* seedlings were used for mRNA extraction. Mean values $\pm$ SD are shown (n = 3). Different lowercase letters above columns indicate a significant difference in relative expression level of a gene among different P treatments (P < 0.05 by Tukey's test).

13
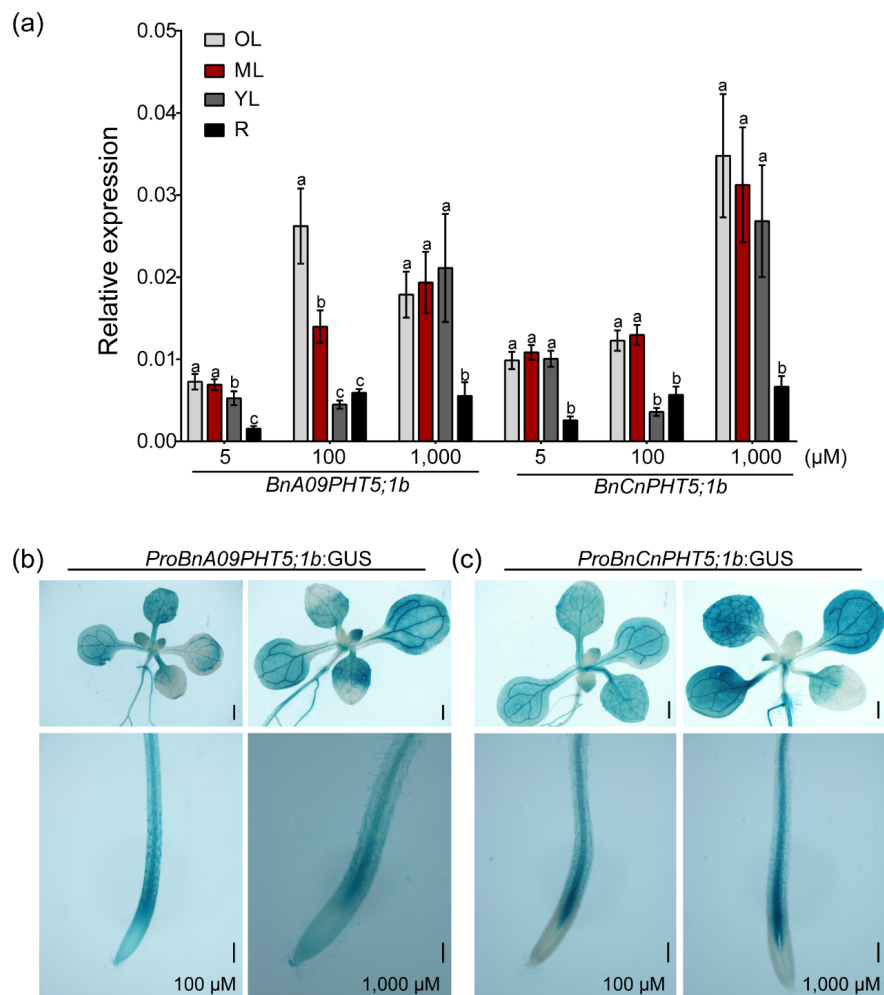
Figure 2. Expression of *BnPHT5;1bs* in *Brassica napus* and *Arabidopsis* organs.

(a) The relative expression of *BnPHT5;1bs* in different organs of *Brassica napus* . 16-day-old *Brassica napus*seedlings grown in hydroponic medium supplemented with 5 μM, 100 μM and 1000 μM P were used. Mean values $\pm$SD are shown (n = 3). Different lowercase letters above columns indicate significant differences among organs of *Brassica napus* cultivar Westar 10 under the same P treatment (P < 0.05 by Tukey's test). OL, old leaf; ML, mature leaf; YL, young leaf. **(b, c)** GUS staining of Pro*BnA09PHT5;1b* :GUS and Pro*BnCnPHT5;1b* :GUS transgenic Arabidopsis (Col-0) plants grown at 100 μM and 1,000 μM P supply. 10-day-old seedlings were used. Bars = 100 μm.

14
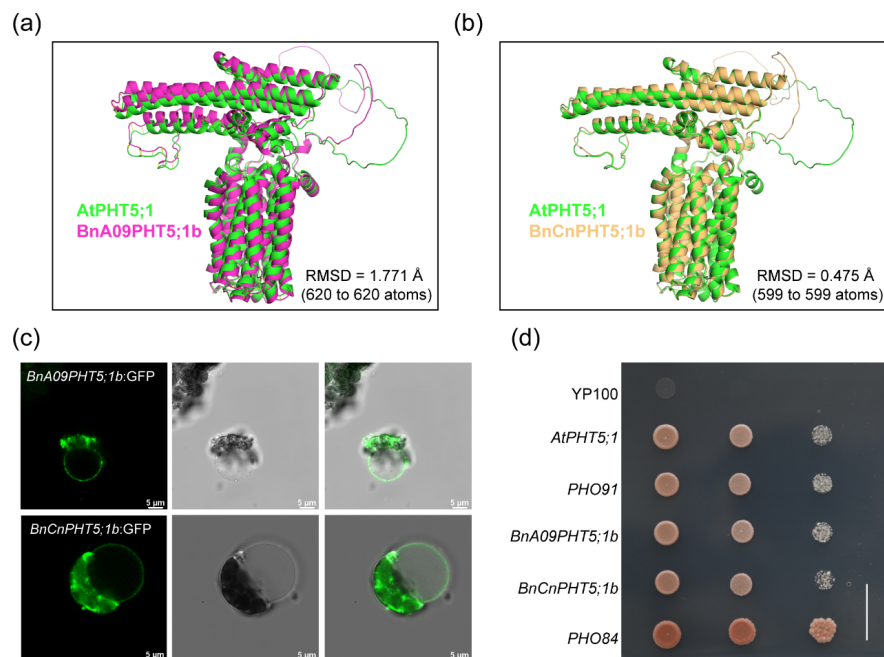
Figure 3. Localization and Pi transport activity of BnPHT5;1b proteins.

(a, b) 3-D structure comparison of BnPHT5;1b proteins and AtVPT1. The Alphafold2 tool was used to predict protein 3-D structure. Pymol was used to calculate the similarity. **(c)** Tonoplast localization of BnA09PHT5;1b and BnCnPHT5;1b. GFP-labeled BnPHT5;1b constructs were expressed in mesophyll protoplast from leaves of 3-4-week old *Arabidopsis* seedlings and the GFP signal was recorded using a Leica SP8 confocal microscope. Scale bar = 5 μm. All experiments were repeated twice, and similar results were obtained.**(d)** BnPHT5;1b confers Pi transport activity in yeast. Constructs including BnPHT5;1b were expressed individually in YP100 (Δpho84Δpho87Δpho89Δpho90Δpho91Δgit1). Strains were diluted to OD600 values of 1, 0.1, 0.01 and dripped on YNB medium (pH 5.6) supplemented with glucose and 30 mM Pi for 5 days incubation at 30 °C. All experiments were repeated three times, and similar results were obtained.
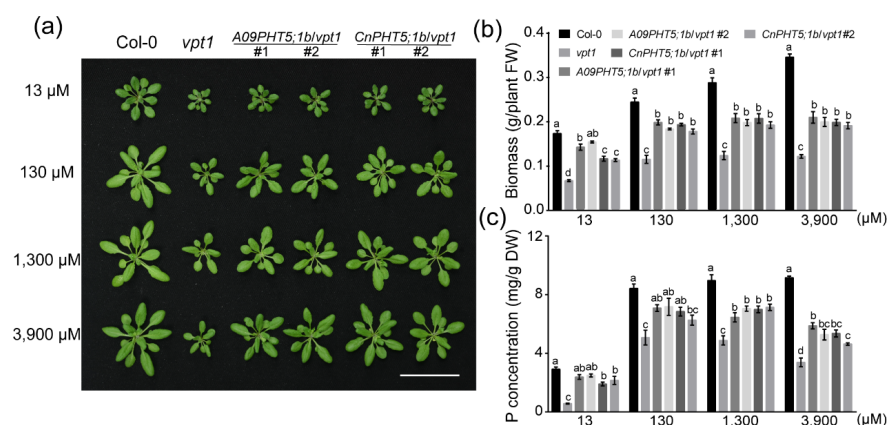
Figure 4. *BnPHT5;1bs* functionally complement *AtPHT5;1* in the Arabidopsis *Atvpt1* mutant at higher Pi supplies.

(a) Phenotype of 4-week-old Col-0, *vpt1* and BnPHT5;1b/*vpt1* seedlings grown with various Pi concentrations. 6-day-old seedlings grown on 1/2 MS (Murashige and Skoog) medium (Murashige and Skoog, 1962) were transferred to ANS solution (Arabidopsis nutrient solution; Liu et al., 2016) supplemented with 13 μM, 130 μM, 1300 μM or 3,900 μM Pi for 3 weeks. Scale bars = 5 cm.(b) Fresh weight and (c) total P concentration of Col-0 (wild type), *vpt1* and BnPHT5;1b/*vpt1* lines in (a). Mean values ±SD are shown (n = 4). Different lowercase letters above columns indicate a significant difference among different lines under each P treatment (P < 0.05 by Tukey's test).
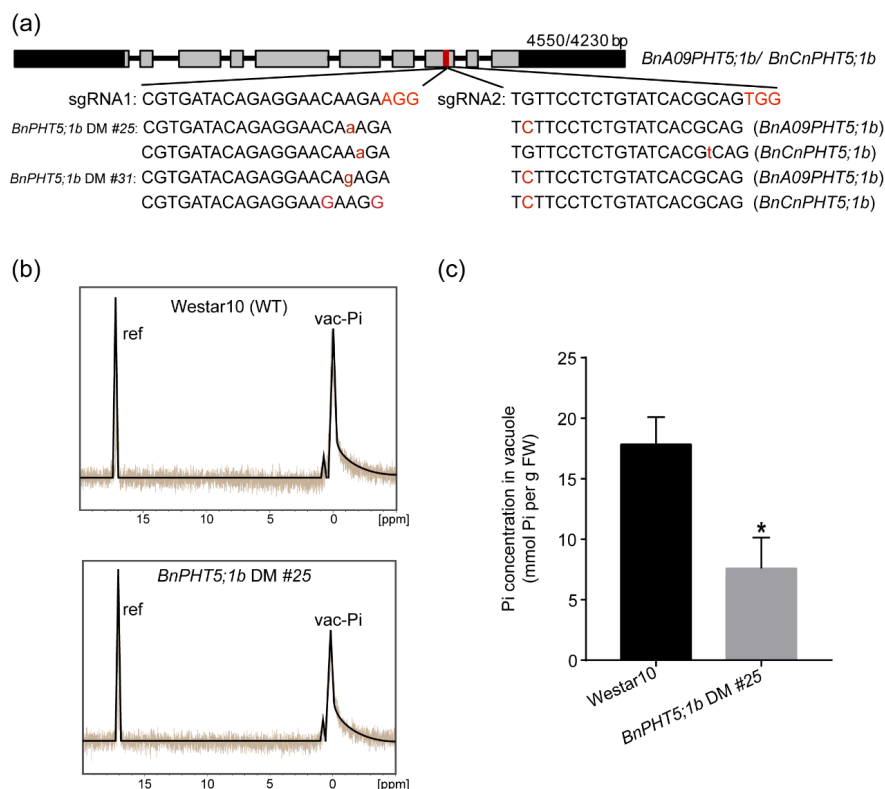
Figure 5. Vacuolar Pi concentrations are significantly reduced in roots of the*Bnpht5;1b* **double mutant.**

(a) *BnPHT5;1b* double mutants with different types of mutation generated by the Crispr-cas9 system. (b, c) Pi concentrations in the root vacuoles of Westar 10 and a *BnPHT5;1b*double mutant (*BnPHT5;1b DM #25*). Plants grown with 100 μM Pi supply were transferred to 1,000 μM Pi for 2 hours before conducting Nuclear Magnetic Resonance (NMR) spectroscopy analysis. Ref, methylene diphosphonate (MDP). Data are mean ± SD (n=3). Asterisks indicate significant differences from control (Student's t-test, * P < 0.05).

16
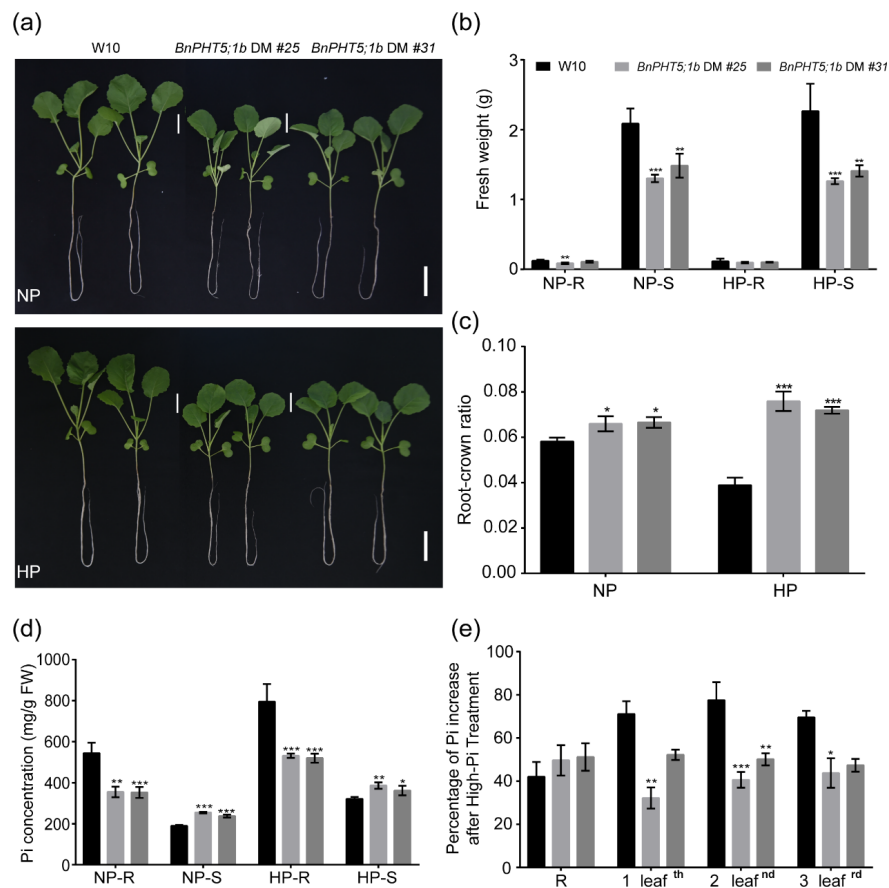
Figure 6. Disruption of *BnPHT5;1b* causes slower growth of *Brassica napus* under P-sufficient and high P conditions.

(a) Phenotypic comparison of W10 and BnPHT5;1b DM lines under Pi-sufficient and high Pi conditions. 10-day-old seedlings grown in Hogland solution containing 100 μM Pi were transferred to 100 μM and 1,000 μM Pi, respectively for 7 days growth. **(b)** The fresh weights, **(c)** root-crown ratios and **(d)** Pi concentrations of seedlings shown in panel (a). **(e)** Percentage increase in Pi concentration in W10 and *BnPHT5;1b* DM plants between 100 μM and 1,000 μM Pi. Data are mean $\pm$ SD (n=4). W10, Westar 10; *BnPHT5;1b DM #25* and *BnPHT5;1b DM #31* , *BnPHT5;1b* double mutants. Asterisks indicate significant differences from control (Student's t-test, * P < 0.05, ** P < 0. 01, *** P < 0.001).

17
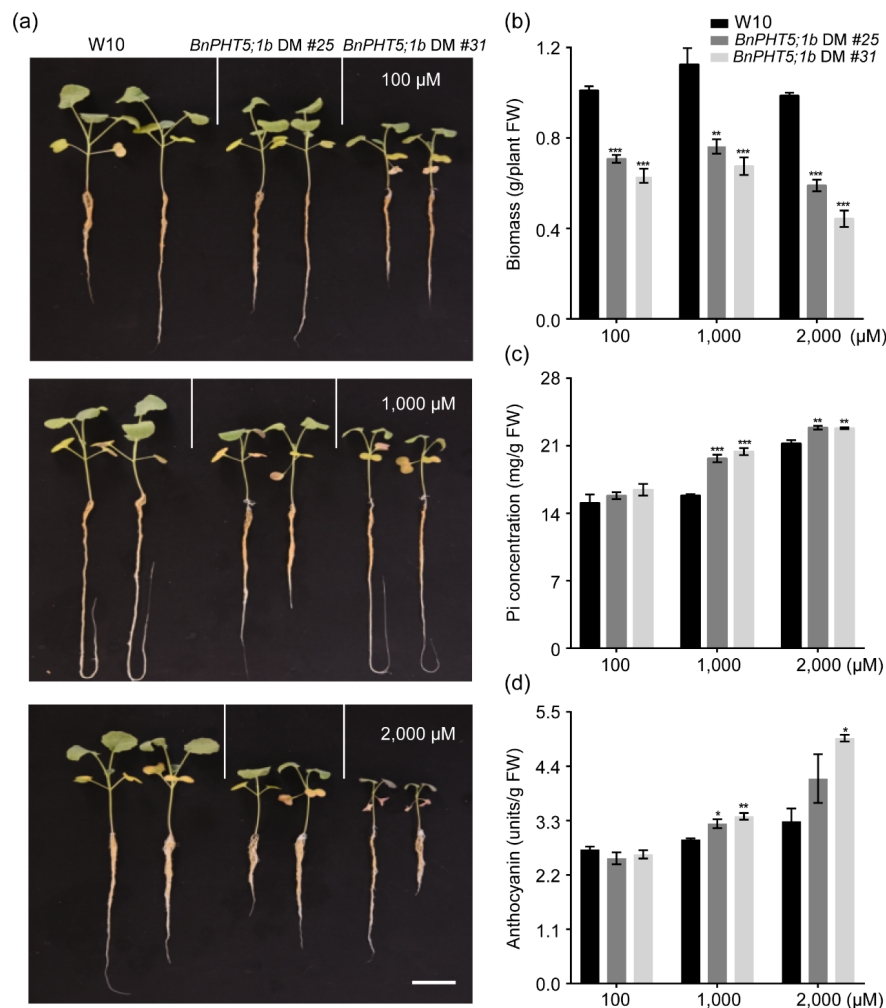
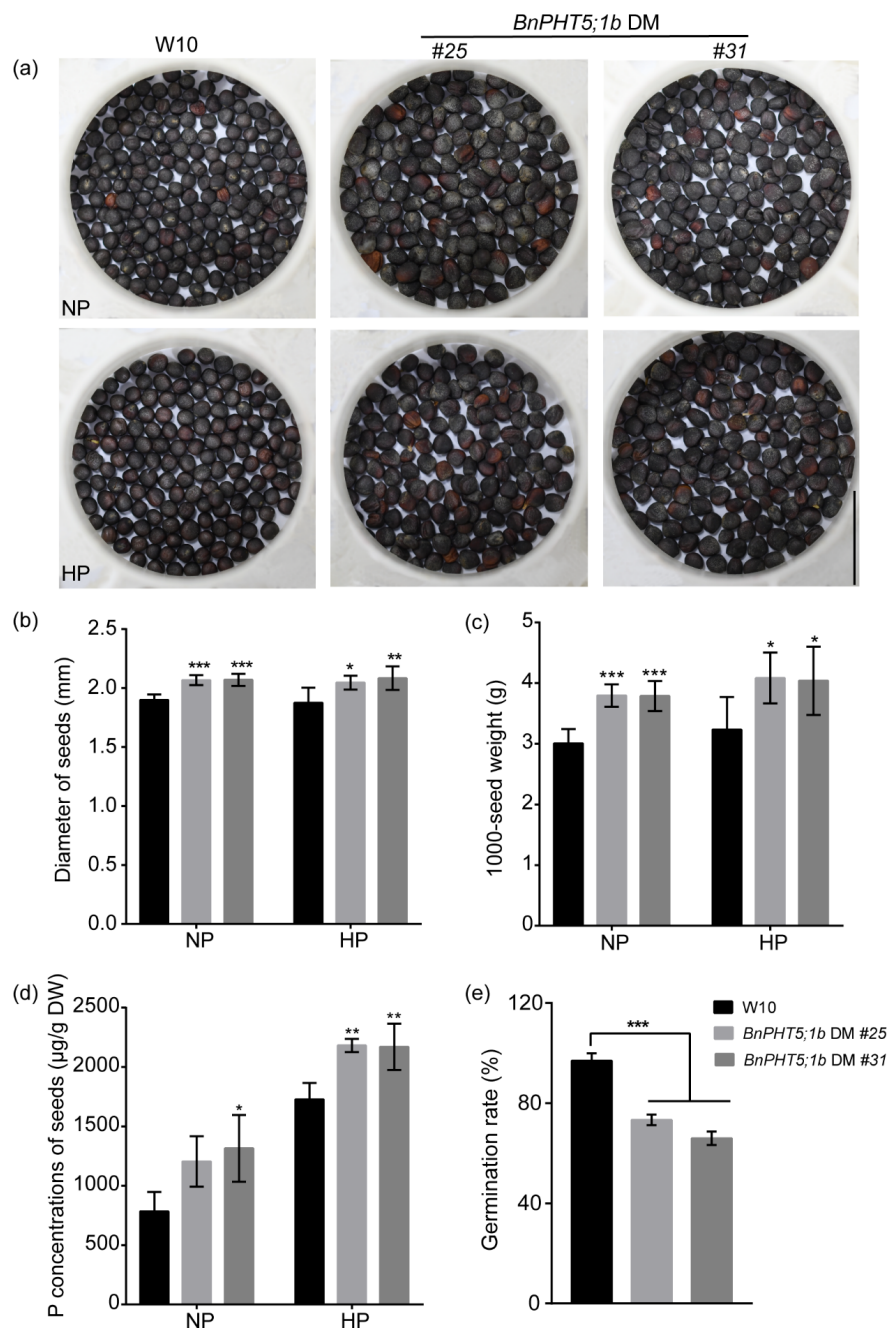**Figure 7. Disruption of *BnPHT5;1b* reduces *Brassica napus* adaptability to fluctuations in Pi supply.**

(a) The phenotype of W10 and *BnPHT5;1b* DM lines. 5-day-old seedlings grown under different Pi supplies (100 μM, 1,000 μM, 2,000 μM) were transferred to media lacking Pi for 14 days. Scale bars = 5 cm. **(b)** Biomass, **(c)** Pi concentration and **(d)** leaf anthocyanin concentration of W10 and *BnPHT5;1b* double mutants following changes in Pi supply. W10, Westar 10, wild type; *BnPHT5;1b DM #25* and *BnPHT5;1b DM #31* ,*BnPHT5;1b* double mutants. Data are mean $\pm$ SD (n = 4). Asterisks indicate significant differences from control (Student's t-test, * P < 0.05, ** P < 0. 01, *** P < 0.001).

18
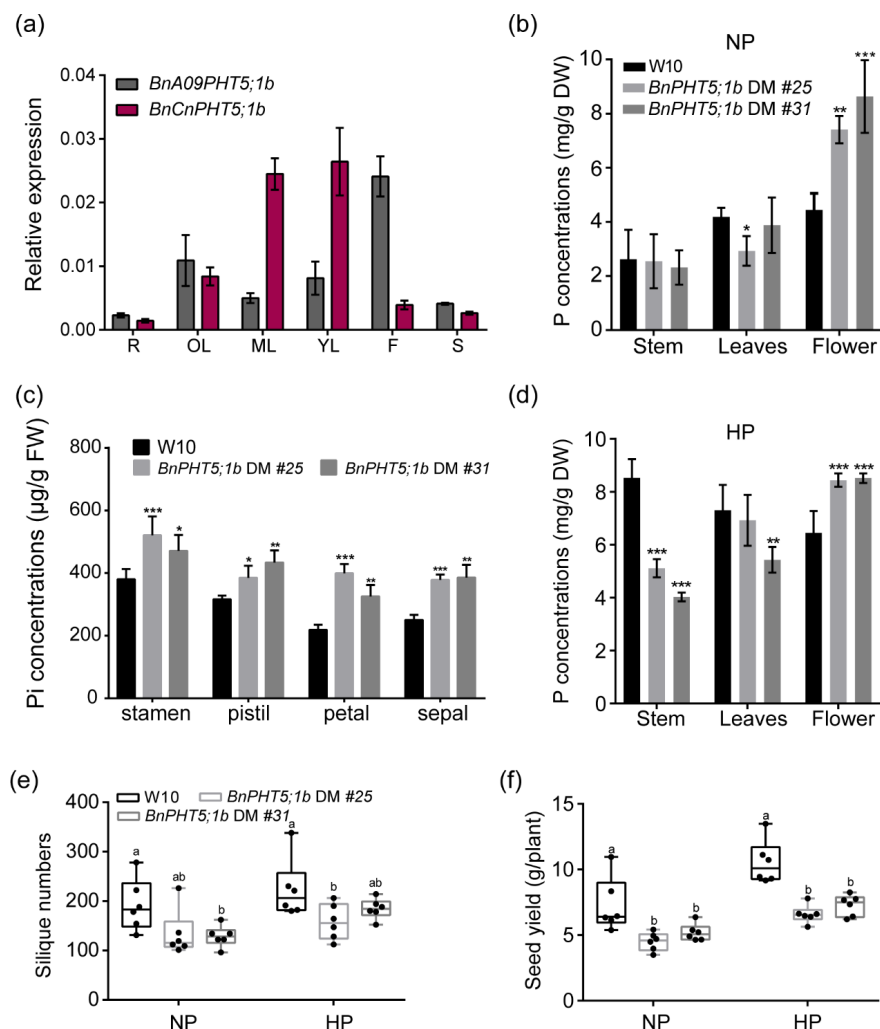
Figure 8. Disruption of *BnPHT5;1b* causes excessive allocation of Pi to the flowers of *Brassica napus* and the reduction of seed yield and silique number.

(a) qRT-PCR analysis of *BnPHT5;1b* expression in various tissues of W10 grown in NP conditions at the flowering stage. *BvEΦ-a* and *BnTubulin* mRNAs were used as internal controls. Data are shown as the mean $\pm$ SD (n = 4). (b-d) Comparison of total P concentrations in the shoot (stem, leaf and flowers) (b) and Pi concentrations in floral organs (c) between W10 and *BnPHT5;1b* double mutants grown in NP conditions and total P concentrations in shoot (stem, leaf and flowers) between W10 and *BnPHT5;1b* double mutants under HP conditions (d). Data are mean $\pm$ SD (n=5). Asterisks indicate significant differences from control (Student's t-test, * P < 0.05, ** P < 0. 01, *** P < 0.001). (e, f) The silique number and seed yield of W10 and *BnPHT5;1b* double mutants grown under NP and HP conditions. Data are mean $\pm$ SD (n=6). Different letters above columns indicate a significant difference among different lines under each P treatment (P < 0.05 by Tukey's test). NP, normal P supply, 150 mg P/kg soil; HP, high P supply, 500 mg P/kg soil. *BnPHT5;1b DM #25* and *BnPHT5;1b DM #31*, *BnPHT5;1b* double mutants.

Figure 9. Disruption of *BnPHT5;1b* affects seeds traits of *Brassica napus* grown under NP and HP conditions.

(A) Seed size of W10 and BnPHT5;1b double mutants. Scar bar= 1 cm. **(B)** Seed diameter; **(C)** 1000-seed weight;**(D)** P concentration of seeds; **(E)** seeds germination rate. Seeds were incubated 6 days in pure water for germination assay. Data are mean ± SD (n=6). NP, normal P supply, 150 mg P/kg soil; HP, high P supply, 500 mg P/kg soil. *BnPHT5;1b DM #25* and*BnPHT5;1b DM #31* , *BnPHT5;1b* double mutants. Asterisks indicate significant differences from control (Student's t-test, * P < 0.05, ** P < 0. 01, *** P < 0.001).

20